Journal of Power Sources 238 (2013) 227–235

Contents lists available at SciVerse ScienceDirect

Journal of Power Sources

journal homepage: www.elsevier.com/locate/jpowsour

# Investigation of anode configurations and fuel mixtures on the performance of direct carbon fuel cells (DCFCs)

Borja Cantero-Tubilla [a,*], Chunchuan Xu [a], John W. Zondlo [a], Katarzyna Sabolsky [b], Edward M. Sabolsky [b,1]

[a] Department of Chemical Engineering, West Virginia University, P.O. Box 6106, Morgantown, WV 26506, USA
[b] Department of Mechanical and Aerospace Engineering, West Virginia University, P.O. Box 6106, Morgantown, WV 26506, USA

## HIGHLIGHTS

- Evaluation of anode configurations and fuel mixtures in a direct carbon fuel cell.
- SEM analysis showed the microstructure of the cell and the porosity of the anode.
- DCFC showed 85 mW $cm^{-2}$ (800 °C) with a dense-porous GDC anode.
- DCFC showed 85 mW $cm^{-2}$ (800 °C) with a 6 vol% Li–K carbonate mixture.
- An equivalent circuit to explain raw impedance data in DCFCs was proposed.

## ARTICLE INFO

*Article history:*
Received 22 October 2012
Received in revised form
12 March 2013
Accepted 15 March 2013
Available online 26 March 2013

*Keywords:*
Direct carbon fuel cell
YSZ
GDC
Carbonates
Percolation threshold
Anode charge transfer resistance

## ABSTRACT

A variety of anode configurations and fuel mixtures were evaluated in a direct carbon fuel cell (DCFC) which was composed of a planar 8 mol% Y2O3-ZrO2 (YSZ) electrolyte with a multilayer (La0.6Sr0.4)0.98(Co0.2Fe0.8)1O3$_{-\delta}$. (LSCF) cathode. A Gd-ceria (GDC) catalyst layer was deposited onto the anode side with various levels of porosity. The fuel composition consisted of solid carbon black mixed with various amounts and compositions of Li, Na, K, and Ba carbonate eutectics. The anode performance was characterized in terms of structure (porosity), catalysts, carbonate content, and carbon composition in the anodic mixture through voltage–current–power density and electrochemical impedance spectroscopy (EIS) measurements, which directly assessed the change in charge transfer resistance in anode as function of alterations in the anode. The best performance was 85 mW $cm^{-2}$ at 800 °C with a cell combining dense-porous GDC anodic structure and 6 vol% Li–K carbonate mixture loading in the anodic chamber. The polarization of this anode configuration was 0.15 Ω cm2 at 800 °C compared to 50.3 Ω $cm^2$ displayed by a bare YSZ electrolyte. Post-mortem characterization by scanning electron microscopy and energy-dispersive spectroscopy showed no effect of carbonate corrosion in the YSZ electrolyte over the time frame of experiments.



## 1. Introduction

Over the past decade, the interest in decreasing greenhouse gas emissions and increasing renewable energy production has gained momentum, but global $CO_2$ emissions worldwide continue to rise due to the rapidly increasing energy demands from emerging economies. The use of coal and biomass will continue to dominate as a global energy source for the near future, until wind, solar, and other truly clean generation sources are fully developed and brought to the world market [1–3]. Thus in the near term, it is essential to develop technologies which utilize carbon fuels as efficiently as possible for generating electricity. There is already considerable interest in clean carbon technologies for electricity production with greenhouse gas sequestration; however, these technologies impose significant energy and cost penalties. In addition, sequestration is only effective on the large scale, limiting possible benefits from distributed power generation. This situation suggests a clear need for alternative or complementary clean carbon technologies [4,5].

The direct carbon fuel cell (DCFC) is a technology that could be utilized to complement large-scale sequestered clean-coal systems [6]. The direct carbon fuel cell has the potential to cleanly convert the

* Corresponding author.
*E-mail addresses:* bcantero@mix.wvu.edu (B. Cantero-Tubilla), Chunchuan.Xu@mail.wvu.edu (C. Xu), John.zondlo@mail.wvu.edu (J.W. Zondlo), Kathy.sabolsky@mail.wvu.edu (K. Sabolsky), Ed.sabolsky@mail.wvu.edu (E.M. Sabolsky).
[1] Tel.: +1 304 293 3272; fax: +1 304 293 6689.

0378-7753/$ – see front matter © 2013 Elsevier B.V. All rights reserved.
http://dx.doi.org/10.1016/j.jpowsour.2013.03.072

chemical energy of solid carbon directly into electricity without a reforming process. Moreover, the need for combustion, gasification or moving machinery associated with conventional electric generators is not required within a DCFC system, which represents a possible economic benefit compared to SOFCs [7]. The DCFC is not dependent upon pure hydrogen fuel which is expensive to synthesize, purify and store. The present world capacity for hydrogen production is currently at a limit which just meets the demand for synthetic fertilizers and petroleum hydrogenation [8–10]. The DCFC can use petroleum coke, coal coke, and gaseous carbon-containing species, as well as biomass-derived carbon (charcoal) [11–13]. Other sources of fuel may include food waste, human waste, wood, switchgrass, corn stover, palm, rice, algae, and sugarcane. The local availability of each of these examples varies depending upon the national (or international) region. Thus, the DCFC could be considered as "locally grown" power devices.

The DCFC offers a greater thermodynamic advantage over other fuel cell types, where the theoretical efficiency is near 80%, much higher than the molten carbonate fuel cell (MCFC) or SOFC running on hydrogen or natural gas (nominal efficiency of 45–60%) [1,14]. The use of coal or other fossil fuels within a DCFC releases no particulates (fly ash); therefore, the reduced emissions permit the use of the technology within confined spaces and urban areas. In addition, the oxidation of carbon in a DCFC occurs electrochemically at the anode without directly mixing with air, and thus the $CO_2$ produced may be nearly pure and free of other contaminant gases such as $SO_x$ and $NO_x$.

However, DCFCs present some issues that have to be addressed before commercialization can begin. The direct carbon fuel cell shows typical open circuit voltages (OCVs) in the range of 1.1–1.2 V, depending upon the anode reaction with solid carbon. The initial OCV may permit a higher current draw from the fuel cell, but because of the concentration polarization occurring at high current densities, the current density is limited to a low range ($<$500 mA cm$^{-2}$), leading to maximum power densities lower than 150 mW cm$^{-2}$ at 800 °C [15]. At high current densities, as the reactant (C in this case) is consumed, there is a loss of potential because of the inability of the surrounding material to maintain a constant bulk concentration forming a concentration gradient. Several processes may contribute to the concentration polarization: slow diffusion of the gas phase in the electrode pores, solution/dissolution of reactants/products into/out of the electrolyte, or diffusion of reactants/products through the electrolyte to/from the electrochemical reaction site, the latter being a major contributor [16]. In the present system, considering that the carbon particles are the reactant, it is the lack of mobility of the carbon particles that leads to the very high polarization losses dominating the total resistance of the cell. Because of the sluggish kinetics of the electrochemical oxidation of carbon, improving the anode kinetics is the key issue for achieving a high performance with DCFCs [15]. In addition, diffusional limitations are present depending upon fuel/anode mixing, which is typically not a problem when utilizing gaseous fuels such as hydrogen. The mechanism of electrochemical oxidation of carbon is rather complicated and the existing literature on this topic is scarce due to the lack of techniques to assess reaction intermediates in molten salts at high temperatures [17,18].

In the last five years, results have been published which address these anode issues and the oxidation mechanism. Zecevic et al. [11] and Cherepy et al. [19] were some of the first groups investigating the use of solid dry carbon as fuel in SOFCs in molten carbonate systems [11]. Regarding the type of carbon fuel, Li et al. [18] (in a computational study) and Chen et al. [20] demonstrated that the performance of the cell shows a strong dependence on the structure of the carbon fuel and its degree of crystallinity, with high surface area carbon black yielding a two-order of magnitude increase in performance over graphite. Li et al. [13] studied the performance of different Australian coals in a direct carbon fuel cell. This assessment showed that $Al_2O_3$ and $SiO_2$ impurities inhibit the anodic reaction, while CaO, MgO, and $Fe_2O_3$ display a catalytic effect on the electrochemical oxidation of carbon. Other authors have investigated performance improvements of the DCFC by adding catalysts to the anode side. Tang and Liu [21] proposed that the electrochemical oxidation of C to $CO_2$ occurs through the formation of CO; therefore, two chemical steps must be catalyzed. They used Gd-doped ceria (GDC) mixed with silver to catalyze the electrochemical oxidation of CO, and an Fe-based catalyst loaded with the carbon fuel to enhance the Boudouard reaction, which produced CO by a reaction of C with $CO_2$. This resulted in an improvement of the cell performance. Li et al. [22] studied the effects of catalytic gasification on the DCFC with a solid oxide electrolyte. The experiments were carried out using K, Ca, Ni as catalysts in carbon black, while controlling the temperatures of the cell between 700 and 1000 °C. The order in catalysis improvement for carbon black gasification with $CO_2$ was K $>$ Ni $>$ Ca. Dudek and Tomczyk. [23] reported that the incorporation of a uniformly dispersed nano-oxide electrolyte into the carbon matrix extends the reaction zone. This work showed that the maximum power density could be increased by a factor of five with 12 wt% GDC and a factor of four with 10 wt % 8YSZ, but the maximum power density achieved for the system was only 2.4 and 1.2 mW cm$^{-2}$ at 700 °C, respectively. These authors also added Ag as catalyst to the carbon load which further improved the performance, but with a very low maximum power density of 4.5 mW cm$^{-2}$ at 700 °C. Ju et al. [24] used a Ni-YSZ anode-supported cell with a YSZ electrolyte and a LSM cathode layer. They loaded the carbon fuel with Sn which plays a major role in both building a favorable bridge between the solid fuel and the solid anode, and facilitating the electrochemical oxidation of carbon to CO, achieving a maximum power density of 105 mW cm$^{-2}$ at 900 °C. Various carbonaceous fuels were tested by CellTech Power using a liquid tin anode solid oxide fuel cell (LTA-SOFC) achieving a maximum power density of 170 mW cm$^{-2}$ on hydrogen and JP-8 (jet fuel) [25,26].

In the present work, planar YSZ electrolyte-supported DCFCs were fabricated with a common multi-layered LSCF cathode. The cells were tested electrochemically to investigate the effect that the anode structure, anode catalytic layer composition and microstructure, carbonate composition, and carbon fuel/carbonate ratio, have on the performance of the cell. The performance of the cells was evaluated by means of the voltage–current–power ($V$–$I$–$P$) curve and the anode polarization by EIS. The previously mentioned works in the literature have discussed a few of these areas individually, but the distinct association of these variables was never solidified, since the $V$–$I$–$P$ performance and the anode characteristics were not directly related to the anode polarization (anode charge transfer), which is of prime importance in this work.

## 2. Experimental

Electrolyte-supported button cells similar to those utilized in SOFC research were fabricated. Since the anode polarization is the prime area of interest within this work, the electrolyte-supported architecture is the proper platform permitting straight-forward alterations to the anode surface and structure. YSZ disks were fabricated from 8YSZ powder (Daiichi Kigenso Kagaku Kogoyo Co., LTD, Japan) with a final dimension of 4-cm diameter and an average thickness of ~190 μm. These electrolyte membranes were prepared by tape-casting and sintering at 1450 °C for 2 h, followed by a forging process at 1400 °C for 6 h. The final electrolyte membranes showed a density of 99% theoretical (measured by the Archimedes method). GDC ink was deposited on both sides of the wafer by

screen-printing using a DEK Model 248, CERD screen printer. GDC powders were synthesized by solid-state reactions using cerium ammonia nitrate and gadolinium carbonate hydrate as the raw materials [27]. The GDC layers had a thickness of 3–7 μm after sintering at 1300 °C for 2 h. The GDC layer on the cathode side acts as a barrier layer to avoid any reaction between the cathode material and the electrolyte at high temperature. As will be discussed later, the GDC layer on the anode side will act as a catalyst layer for enhancing the electrochemical oxidation of carbon. For some cells, an extra layer of GDC was printed over the initial thin layer on the anode side, which contained rice starch as a pore former (50–50 vol %). The final second porous GDC layer displayed an average thickness of 50 μm. The active cell area was 2.85 $cm^2$ in the center of the YSZ membrane. On the cathode side of the cell, the active GDC-LSCF layer was screen-printed and dried at 60 °C for 20 min prior to the screen-printing of a pure LSCF current collector layer over the previous layer. The average thickness of the active layer was 5–8 μm, while for the current collector layer the thickness was ~17–21 μm. The LSCF powders were synthesized by attrition milling and calcination at 1100 °C for 2 h in air with the raw cation sources being $La_2O_3$, $SrCO_3$, $CoCO_3$, and $Fe_2O_3$. The active and current collector layers are sintered together at 1000 °C for 2 h in air. A scanning electron micrograph (SEM, Hitachi S-4700) of the cell cross-section thus fabricated is shown in Fig. 1.

The different anodic compositions in the present study utilized various mixtures of carbonates mixed by ball-milling with the base-line carbon black fuel [1,20] at different ratios: 0, 2.5, 6, 9.5, 13, and 22 vol % carbonates/carbon. The carbonate combinations of $Li_2CO_3$–$Na_2CO_3$, $Li_2CO_3$–$Na_2CO_3$–$K_2CO_3$, $Li_2CO_3$–$BaCO_3$, $Na_2CO_2$–$K_2CO_3$, and $Li_2CO_3$–$K_2CO_3$ were considered in this study. All the carbonate mixtures were the eutectic composition for each system (i.e., Li (41 wt %) + Na (59 wt %), Li (32.5 wt %) + Na (32.9 wt %) + K (34.6 wt %), Li (37 wt %) + Ba (63 wt %), and Na (53 wt %) + K (47 wt %)) except for the $Li_2CO_3$–$K_2CO_3$ mixture [28,29]. The composition was slightly different from the eutectic (68 mol % $Li_2CO_3$ (53 wt %) + 32 mol % $K_2CO_3$ (47 wt %)) in order to compare against performance data obtained in previous papers by Jiang and Irvine [1].

Each single cell was sealed between a 4-cm outside diameter and 2-cm inside diameter alumina tube and an alumina washer of the same dimensions using a mica ring and Aremco Ceramabond® cement, with the anode side bonded within the tube. The cell was loaded with the dry powder anodic mixture until it occupied approximately 2/3 of the volume of the alumina tube. The sealed fuel cell was placed into a Lindberg vertical tube furnace and heated to 650 °C while flowing preheated argon (30 sccm) and air (50 sccm) to the anode and cathode chambers, respectively. The electrochemical testing was performed at 650, 700, 750, 775, and 800 °C. The temperature of the cell was measured on the anode side by a type K thermocouple placed just above the carbon/carbonate mixture. A cross-section of the testing set up is shown in Fig. 2 [30]. Silver mesh and wire were attached to the cathode surface with LSCF ink for current collection. Platinum mesh was placed on cell's surface in the anode chamber (on top of the YSZ electrolyte, GDC dense layer, or GDC porous layer depending on the experiment). It was used for current collection at the anode. A single drop of platinum ink was used to assure good contact between the platinum mesh and the anode surface. The electrochemical characterization of the cell was carried out using a galvanostat/potentiostat (Solartron 1280Z, Solartron Analytical, England) with a frequency response analyzer (impedance/gain-phase analyzer Solartron 1260, Solartron Analytical, England). The *V–I–P* plot was constructed by applying constant current that increases stepwise at 2 mA $s^{-1}$ using an electronic load. The measurement proceeded until the cell voltage reached 0 V. The EIS measurements were carried out at open circuit voltage and under a variety of discharging currents. The impedance spectra were measured through the input of a perturbed sine wave with the amplitude of 10 mV within the frequency range of 20 kHz–10 mHz. Analysis and curve fitting of the data were processed by the assembled software ZPlot® and ZView™ for Windows (Scribner Associates Incorporated). After electrochemical testing, the cell was cooled in argon to room temperature. SEM with energy dispersive spectroscopy (EDS) was used for the post-mortem characterization of the microstructure and composition of the anode.

The anode polarization resistance (or more specifically, the charge transfer resistance) of the different cells was assessed by means of a novel deconvolution model. The contribution of the electrolyte to the polarization resistance of the entire cell was subtracted by considering the ohmic resistance of the cell at the origin of the Nyquist plot. To quantify the polarization resistance of just the anode, the cathode polarization resistance was subtracted from the polarization resistance of the entire cell (second intersection of the raw impedance data with the real axis). The cathode polarization resistance was quantified using a symmetric cell, with the same multilayer cathode printed on both sides of the electrolyte, and a Pt reference electrode on one side. Since every cell incorporates the same multilayer cathode processed with the same procedure, the same cathode polarization resistance was assumed for every cell.

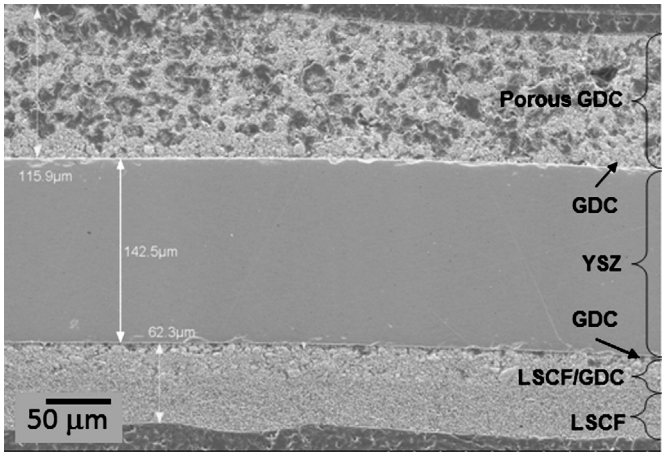


**Fig. 1.** Cross-sectional SEM micrograph of a non-tested direct carbon fuel cell with a YSZ solid electrolyte.

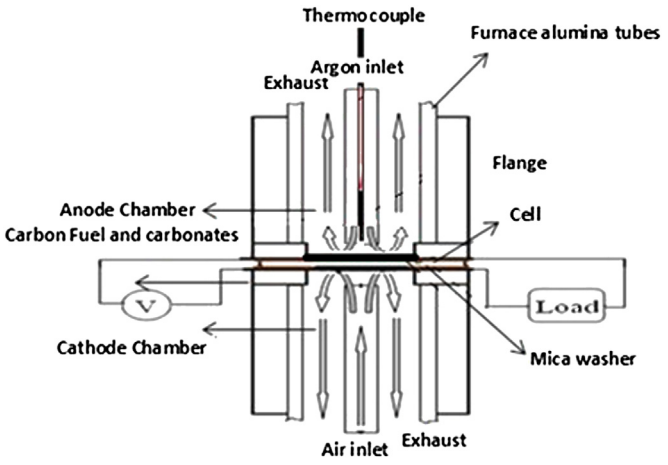


**Fig. 2.** A cross-section representation of the testing set up for the direct carbon fuel cell.

## 3. Results and discussion

### 3.1. Anode catalyst microstructure and composition

The goal of these initial experiments was to investigate the influence of the anode configuration on the overall cell performance and the anode polarization resistance for DCFCs operating with carbon black as the fuel. With respect to the anode structure, three options were considered: 1) bare YSZ electrolyte (without any catalyst printed on the anode side), 2) GDC dense layer screen-printed onto the YSZ electrolyte (sintered at 1300 °C), and 3) option number 2 with an additional porous GDC layer (GDC-rice starch ink) screen-printed onto the GDC dense layer and co-sintered at 1300 °C with rice starch providing porosity to the layer. Fig. 3 displays a SEM micrograph of the top-down view of the GDC porous film after thermal treatment at 1300 °C for 2 h. This micrograph shows how the removal of the fugitive rice starch during thermal processing results in a uniform porosity throughout the microstructure with pores and grains in the size range of 1.5 microns. The average porosity of this microstructure is measured to be 35% (SEM image processed with ImageJ software). For these experiments, the anodic mixture was composed of carbon black mixed with the Li and K carbonate composition (68/32 mol %). The total carbonate/carbon mixture consisted of 6 vol % carbonate and 94 vol % carbon in the dry state. This composition corresponds to 20 wt % carbonate in the anodic mixture and has been widely tested in previous studies [1].

Fig. 4 shows the *V–I–P* curves for the cell using the combined dense and porous GDC layers (option 3) as the anode configuration at 650, 700, 750, 775, and 800 °C. It is observed for this particular architecture that the cell power density and the current density increased as expected with temperature as a result of the increased oxygen ion diffusion and exchange kinetics. By increasing the testing temperature from 650 to 800 °C, the current and power density increased five times and the OCV increased by 15%. There is no noticeable increase in cell performance after 775 °C. Fig. 5 shows the maximum power densities (mW $cm^{-2}$) of the cells using each of the three anode configurations. It is observed that the electrochemical oxidation of carbon depends to a great extent on the presence of the GDC catalyst layer on the anode side and its porosity. The maximum power density of the cell tested using no GDC catalyst layer was 7 mW $cm^{-2}$, regardless of the testing temperature. The addition of the dense GDC within the anode resulted in an increase of cell maximum power density by more than 500% reaching a maximum power density of 38 mW $cm^{-2}$ at 800 °C.

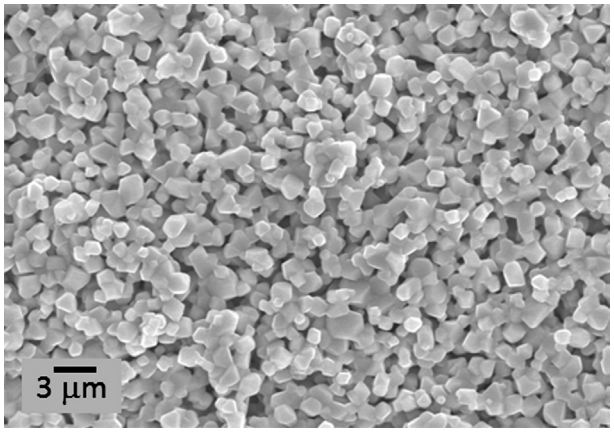


**Fig. 3.** SEM micrograph of the top surface of the porous GDC anode. The porosity within the structure is created by the burnout of rice starch added to the deposited GDC ink.

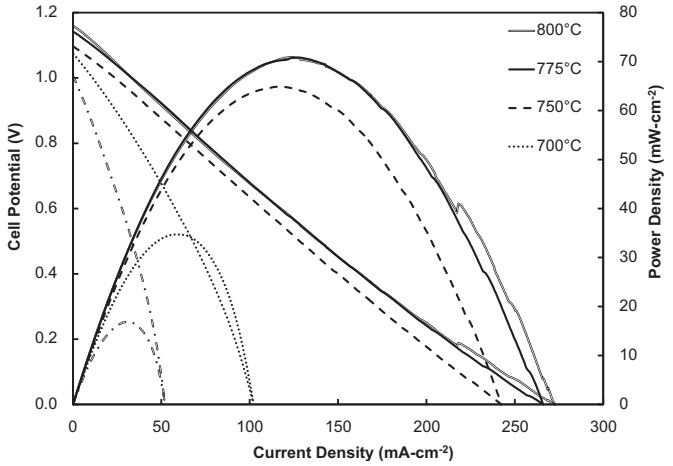


**Fig. 4.** *V–I–P* curves for the cell having the dense/porous GDC anode structure, tested with a (Li–K) carbonate concentration of 6 vol%.

Upon adding the additional porous GDC catalytic layer over the dense layer, the performance of the cell increased 200% (~70 mW $cm^{-2}$ at 800 °C) over the performance of the pure dense GDC layer. Overall, the GDC bilayer structure increased the performance over the bare YSZ electrolyte by 1000%.

The addition of the GDC layers enhances the performance of the cell in several ways. The GDC potentially provides a more active catalytic GDC/carbonate interface for the solid carbon electrooxidation. The porosity in the GDC layer also assists in increasing the surface area of the electrode, and therefore, the triple phase boundary (TPB) region what is considered to be the system GDC (ionic conductor)/C (electronic conductor and fuel). High performance anodes require a sufficient concentration of TPBs, where the fuel and oxygen ions come into contact along with ample electrical conduction paths. Such a high concentration of TPBs can be obtained using mixed ionic-electronic conductor (MIEC) materials exhibiting sufficiently high porosity. Therefore, this study shows that the electrochemical oxidation of carbon occurs at the junction of the ionically-conducting GDC, the porosity filled with the percolated network of carbon acting as the electronic conductor,

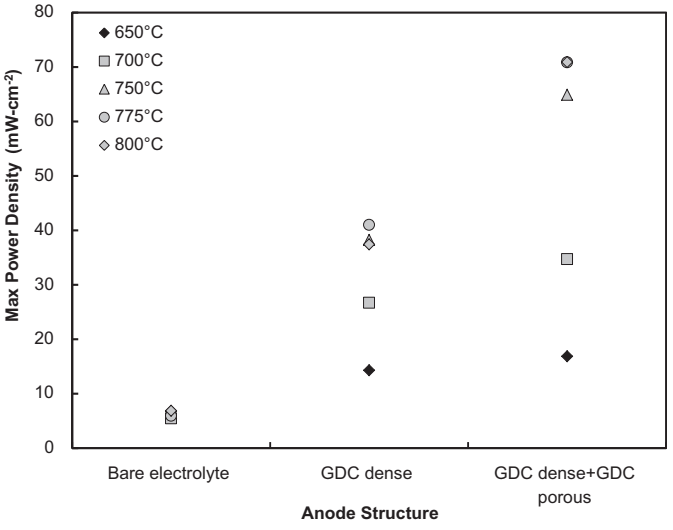


**Fig. 5.** Maximum performance of the different cells using different anode structures (bare electrolyte, dense GDC layer on the anode side, combination of dense/porous GDC layers on the anode side). The result for the GDC dense + GDC porous structure was reproduced. These cells were tested using a carbonate (Li–K) concentration of 6 vol%.

and the carbon fuel. In addition, the porous electrode layer must possess enough open interconnected porosity to allow for fuel and product transport at the anode interface, especially at high current densities in order to decrease the concentration polarization of the electrode. In the case of SOFCs, approximately 30 vol % of open porosity is required to facilitate the transport of fuel and product gases [31,32]. In the present work, as shown at high current densities for each temperature in Fig. 4, the concentration polarization of the system is negligible which suggests that the carbon particles are small enough (2.4 μm) and have enough mobility to migrate at a useful rate through the porous GDC and react with the oxide ions at the surface of the GDC layer. Therefore the porosity of the GDC increases the number of active sites for the electrochemical oxidation of carbon. The GDC may also prevent the formation of stable or metastable inorganic phases at the anode/electrolyte interface. It has been reported that the YSZ-based membranes and lithium carbonate react irreversibly to form lithium zirconate at 750 °C [33] which explains why the performance of the cell does not increase at higher temperatures due to the increased ionic conductivity of YSZ. On the other hand, GDC has been used as a composite electrolyte with Li, Na, and K carbonates in intermediate-temperature SOFCs, showing better resistance than YSZ against reaction with carbonates [34,35]. SEM/EDS investigation of both cells run with and without GDC layers showed no presence of K within the electrolyte material after operating in the carbonate solution for >48 h (Li cannot be detected by EDS). Although this investigation does not indicate gross degradation at the electrolyte interface, it cannot discount potential reactions at the nano-level which may disrupt the electrochemical mechanisms.

The *V–I–P* performance was confirmed by the measurement of the anode polarization resistance through EIS for the three anode configurations tested. The EIS spectra for the three anode compositions measured with the mixture and 6 vol % Li–K carbonate and carbon fuel at 800 °C are shown in Fig. 6. The spectra indicate a large ohmic resistance for the cell only with the dense GDC layer. It is suggested that this behavior is caused by a deficiency of wetting of the electrolyte layer by the anodic mixture, therefore, having a true active area smaller than expected. This point was confirmed upon observation of the post-mortem cell, where two regions could be distinguished in the anode. One section of the anode had the anodic mixtures in the form of powders (where the carbonates had not melted during test). On the other hand, chunks of granulated material were found on the other section of the anode, suggesting the wetting of the anode occurred at that section. The EIS data were analyzed using equivalent circuit models to define the various resistance contributions to the overall anode polarization [36]. The typical equivalent circuit for a fuel cell is shown in Fig. 7a where the electrolyte contribution to the impedance is modeled with a resistor $R_1$ (ohmic resistance), the anode and the cathode contributions are modeled by a parallel circuit consisting of a capacitor and a resistor, both in series with the electrolyte resistor ($C_1$, $R_2$ and $C_2$, $R_3$).

From the visual inspection of the raw impedance data in Fig. 6 (OCV 800 °C), there are two clear zones in evidence. At high frequency, there is an elliptical zone representing kinetically controlled processes, and at low frequencies there is a linear zone representing diffusion controlled processes occurring at the anode side of the cell [17,18,37]. The latter is assumed to be caused by diffusion limitation of oxide ions at low frequencies. The most common element describing the diffusion limitation is the Warburg element which models semi-infinite linear diffusion, i.e., unrestricted diffusion to a large planar electrode [36]. The equivalent circuit shown in Fig. 7b (where the combination of R2 and W1, the Warburg element, represents the anode polarization resistance) was used to fit the experimental data of several fuel cells (as will be discussed in the next subsections). However, when fitting the data to this equivalent circuit, the errors were higher than 200%. This poor fit could be explained by the use of capacitances instead of constant phase elements. Obviously, this model is not a good representation of the DCFC impedance data. It was noted that impedance spectroscopy for corrosion phenomena has similar behavior as for the DCFC. Therefore, an equivalent circuit for fitting corrosion data was used here for the DCFC as shown in Fig. 7c (where the parallel combination of R2 and R3 is defined as charge transfer resistance, and, when including the Warburg element parallel to R3, the combination is the anode polarization resistance). An example of the values for the fitted parameters for the

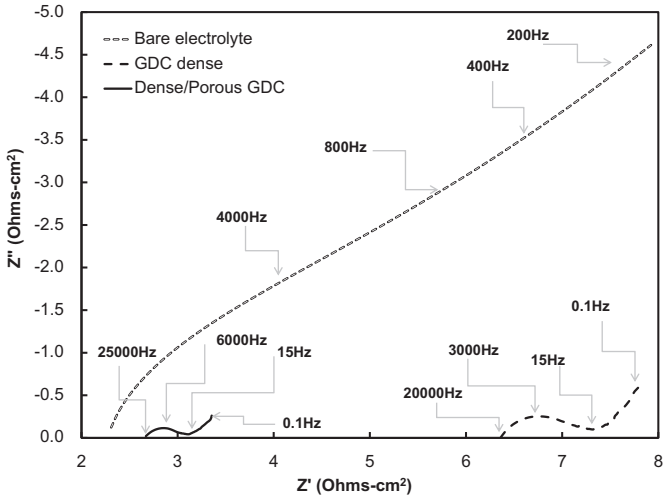


**Fig. 6.** EIS data of the cells at OCV with different anode structures (bare electrolyte, dense GDC layer on the anode side, combination of dense/porous GDC layers on the anode side) at 800 °C.

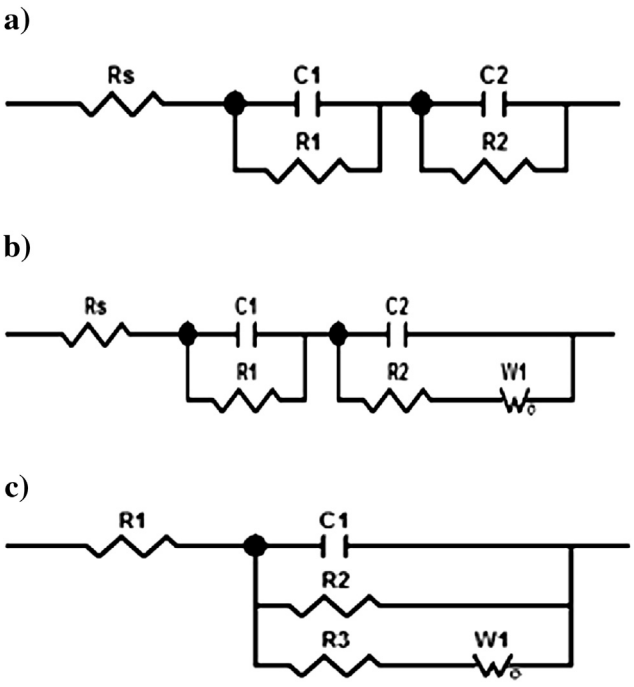


**Fig. 7.** a) Typical equivalent circuit for a fuel cell; b) Typical equivalent circuit of a fuel cell with diffusion controlled processes seen at low frequency; c) Best fit equivalent circuit for the studied direct carbon fuel cells. The error between the impedance data generated by the proposed equivalent circuit and the real impedance data is ~10%.

**Table 1**
Value of the fitted parameters of the equivalent circuit used to model the cell tested with GDC dense/porous layer in the anode, 6 vol% Li–K carbonates using Solartron Zplot software. The ohmic resistance R1 was fixed because it can be determine directly from the Nyquist plot as the first intersection of the raw impedance data with the real axis at high frequency. Resistances in Ohm·cm$^2$, and capacitance in F cm$^{-2}$.

| Element | Value | Error% |
|---|---|---|
| R1 | 5.75 | N/A |
| C1 | 0.00103 | 8 |
| R2 | 6.126 | 1 |
| R3 | 0.0742 | 9 |
| W1–R | 1.66 | 3 |
| W1–T | 0.3235 | 4 |
| W1–P | 0.3868 | 1 |

cell tested with dense/porous GDC layer in the anode, 6 vol % Li–K carbonates are shown in Table 1. The result of the fitting was very close to the experimental data, with a maximum error for the different elements of the circuit of 10%. However, as the equivalent circuit depicted in Fig. 7b had a very clear physical analogy with the mechanisms occurring in a DCFC, the equivalent circuit proposed in Fig. 7c is more difficult to interpret. From Fig. 7c, the parallel combination of R2 and R3 known as charge transfer resistance of the anode. When including the Warburg element, it is the anode polarization resistance. Zeng et al. [38] employed this model for metal salt corrosion controlled by the diffusion of oxidants in the melts. This kind of diffusion-controlled reaction has a typical impedance spectrum with a semi-circle at high frequency and a line at low frequency, which is described nicely by the equivalent circuit in Fig. 7c. More study is necessary to relate the equivalent circuit proposed in Fig. 7c with the real physical behavior of the DCFC operating with carbonates, where corrosion of the electrolyte is suggested by the present data and model.

From Fig. 6, the charge-transfer resistance of the cell with no catalyst printed on the anode side is two orders of magnitude higher at 800 °C than that for the samples with catalyst printed on the anode. This observation agrees with that of Dudek and Tomczyk [23]. The difficulty in transporting oxygen ions in the anode side, where the contact is made with the solid carbon, and the formation of secondary phases at the anode/electrolyte interface [33], could be responsible of the high charge-transfer resistance in the samples with no anode catalyst.

To evaluate further the effect of temperature on the polarization resistance of the cells with the porous/dense GDC anode structure, the ohmic resistance was subtracted from the total resistance obtained from the slope of the polarization curves near OCV in Fig. 4 for the different temperatures. These results are shown in Table 2, where a decrease in every cell resistance is observed as the temperature increases, with a plateau starting at 750 °C. This behavior may be caused by the formation of metastable phases from reaction between the carbonates and YSZ [33]. Since the low cathode polarization resistance measured with the symmetric cell (0.52 and 0.085 Ω cm$^2$ at 650 and 800 °C respectively) can be considered negligible, the polarization resistance of the DCFC is mainly caused by the anode side.

**Table 2**
Values of the total resistances (slope of the polarization curves near OCV), ohmic resistances, and polarization resistance for the DCFCs tested using GDC dense/porous layer in the anode, 6 vol% Li–K carbonates at the testing temperatures.

| Temperature (°C) | Total resistance (Ohms·cm$^2$) | Ohmic resistance (Ohms·cm$^2$) | Polarization resistance (Ohms·cm$^2$) |
|---|---|---|---|
| 650 | 12.3 | 7.7 | 4.6 |
| 700 | 6.5 | 4.9 | 1.6 |
| 750 | 3.9 | 3.1 | 0.8 |
| 775 | 3.5 | 2.8 | 0.7 |
| 800 | 3.4 | 2.7 | 0.7 |

### 3.2. Carbonate-carbon fuel ratio

The anode consisting of a dense GDC layer screen-printed on the electrolyte, and a porous GDC layer printed on the dense GDC layer (option 3 as described above) was selected for all the subsequent testing since this configuration gave the best performance of the three options. The Li–K carbonate mixture was selected again for this set of experiments (68 mol % $Li_2CO_3$/32 mol % $K_2CO_3$), but the ratio of the salt to the carbon fuel was varied. The main role of the molten carbonate solution is to uniformly wet the carbon fuel and electrolyte, which would provide a medium for carbon transport and electrochemical reaction. It is assumed that the carbonate solution contributes to the percolation network of carbon particles that act as the conductive phase for transport of electrons to the current collector from within the solution [35]. Also, the liquid carbonates have been proven useful in wetting the carbon particles over the anode active area, therefore increasing the electronic conductivity of the anode.

Previous investigation showed that in the anode compartment, the carbon particles in direct contact with the electrolyte react with $O^{2-}$ ions producing carbon dioxide and releasing electrons. Carbon dioxide and electrons are also produced by direct reaction of carbon particles in the bulk of the anode solution with $CO_3^{2-}$ ions [39]. Some experiments were performed with the Pt mesh current collector immersed in the bulk of the carbonate solution (and not physically attached to the anode surface). The performance of these cells was much lower than the cells with the Pt mesh attached to the anode, proving the oxidation of carbon takes place at the junction of the GDC and the solid carbon. Away from the GDC layer, carbonate ions participate in another reaction pathway, where they are electrochemically reduced by the carbon fuel within the anodic mixture thereby producing carbon dioxide and electrons. Carbonate ions can also form an equilibrium to produce carbon dioxide and oxide ions, that could also oxidize carbon. It is suggested by Cooper's research that the equilibrium constant of the carbonate dissociation under these experimental conditions, is negligible. When comparing it with the flow of oxide ions produced in the cathode, and considering the low ionic conductivity of carbonates, the low performance of the cells with current collection in the bulk of carbonates is explained [40].

Jiang et al. recently demonstrated attractive DCFC performance for the Li–K system with a NiO-YSZ catalyst layer, utilizing a traditional NiO-YSZ anode-supported SOFC [1]. The same Li–K system was utilized in the present work for a catalyst layer consisting of the porous/dense GDC double-layer discussed above. Different carbonate compositions in the dry state were studied in this work; these compositions were 0, 2.5, 6, 9.5, 13, and 22 vol % carbonates (0, 10, 20, 30, 40, and 60 wt %). This concentration is important, as observed in Fig. 8 which shows the maximum power density (in mW cm$^{-2}$) with the different Li–K carbonate-to-carbon fuel ratios for the anodic mixture at the testing temperatures of 650 °C–800 °C. In addition, depending on the concentration of carbonate, the DCFC will most likely transition from a liquid/solid phase reaction mechanism to a solid/solid and/or solid/gas phase mechanism at the anode. This change in reaction mechanism will be dependent upon the distribution of the carbonates in the anodic mixture, since the percolation of the carbonates will control the probability of forming a liquid solution within the anode compartment during testing. In this work, the carbon black fuel

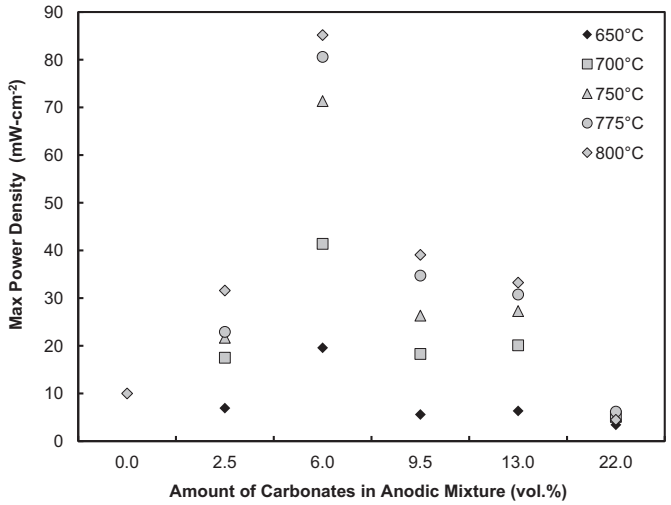


**Fig. 8.** Maximum performance of the cells using different volume fractions of carbonate within the anodic mixture (0, 2.5, 6, 9.5, 13, 22) at various temperatures. These cells were tested with carbon black as the fuel in the anodic mixture, Li–K carbonate and dense GDC/porous GDC layers as the anode structure.

showed a low tap density (0.2 g $cm^{-3}$) which is expected for most similar carbon sources. When the volume fraction of the carbonates is above the percolation threshold, then the probability of contact between the carbonates is high, leading to the formation of the liquid phase. An increased volume of liquid carbonates increases diffusional limitations of the carbon fuel to the electrode, and thus limits the electrochemical oxidation, as observed at low frequencies in the EIS studies. Below the percolation threshold for the carbonates, the carbonates would act as "localized catalysts" for carbon fuel reforming, and the oxidation process would be more similar to that of a SOFC functioning on solid carbon fuel with the GDC working as an ionic conductor and the Pt paste and carbon particles as the electronic conductor. There may be a small probability that a carbonate liquid may form in select areas throughout the anode, which could result in a mixed oxidation mechanism (solid-state, solid/gas or solid/liquid). The Li–K carbonate composition here has a melting point of 576 °C [28]. These assumptions about the carbonate liquid phase formation at the testing temperature, and its dependence on the carbonate concentration, were empirically confirmed upon observation of the anodic mixture after cell testing. At carbonate concentrations of 6, 9.5, 13, and 22 vol %, the anodic mixture was an agglomerate of carbon particles ("chunks of material") in the region close to the GDC electrode, which implies the presence of a liquid carbonate phase at testing temperatures (these agglomerates are slightly observed at 6 vol %, and increase in volume with increasing amount of carbonate). At carbonate concentrations between 0 and 2.5 vol %, the anodic mixture retains its powdery appearance even close to the GDC electrode, suggesting that no liquid phase has been formed.

The performance trend with composition observed in Fig. 8 will be described for the case at 800 °C, but these trends are similar for all temperatures. The highest power density was measured to be 85 mW $cm^{-2}$ for the 6 vol % carbonate addition to the 94 vol % (20 mol %) carbon black fuel at 800 °C. The results obtained in the present work using the porous/dense GDC layer as the anode were higher than the 50 mW $cm^{-2}$ obtained by Jiang and Irvine using a Ni-cermet anode-supported SOFC with a 20 mol % carbon fuel in Li–K carbonates at 800 °C [1]. The 20 mol % carbon in this work is near or below the percolation threshold (~9 vol %) for the carbonate particles within the mixture, depending upon the particle packing efficiency.

The theoretical calculation for the percolation threshold was based on the model developed by Malliaris and Turner for binary systems, and extended to ternary systems in the present work [41]. In this calculation, the carbon black and porosity were considered a single phase with an average particle size of 2.4 μm. The average particle size of the Li and K carbonates (2.6 and 11.3 μm, with 90% of the particles below 21 and 20 μm respectively) was measured by light scattering (Malvern Mastersizer 2000) and confirmed using SEM imaging. With the measured particle sizes for the components, the estimated percolation threshold was found to be 8.7 vol % carbonates with hexagonal packing (coordination number 6), 10.7 vol % carbonates with square packing (coordination number 4), and 13.6 vol % with triangular packing (coordination number 3). This indicates that at carbonate loadings <8.7 vol %, the probability of liquid formation is low, since the melting temperature for the individual carbonates is well above the testing temperature [28]. Therefore, the electrochemical reaction will consist of a mixed solid/solid and solid/gas mechanism, which appears to show the highest kinetics between 6 and 9.5 vol % carbonate addition. As shown in Fig. 8, for carbonate loadings <6 vol %, the maximum power density displays a significant drop in performance to ~20 mW $cm^{-2}$ and ~10 mW $cm^{-2}$ at 2.5 vol % and 0 vol % carbonates, respectively. It appears that the additional Li–K carbonates are acting as a catalyst for the carbon electro-oxidation process.

Fig. 9 shows the charge transfer resistance (as previously defined) of the cells assessed for the different volume percent of carbonate within the anodic mixture (2.5, 6, 9.5, 13, 22%vol) at 800 °C. The charge transfer resistance in the anode was estimated from a full cell EIS scan and this data were fitted to the previously described equivalent circuit (fitted to 10% error). The ohmic and cathode polarizations were subtracted from the EIS scan. The plot shows a significant decrease in charge-transfer resistance in the anode from the 2.5 vol % to the 6 vol % loading, with the anode polarization decreasing from ~1.2 Ω $cm^2$ to ~0.15 Ω $cm^2$, respectively, at 800 °C. The electrolyte/anode interface consisted of the GDC catalyst bi-layer (porous/dense layers), as discussed in the previous subsection. As the carbonate concentration was increased above the percolation threshold of 8.7 vol %, the anode charge-transfer resistance increased significantly (Fig. 9), with the maximum power density also decreasing accordingly. By slightly increasing the carbonate concentration to 9.5 vol %, the charge-

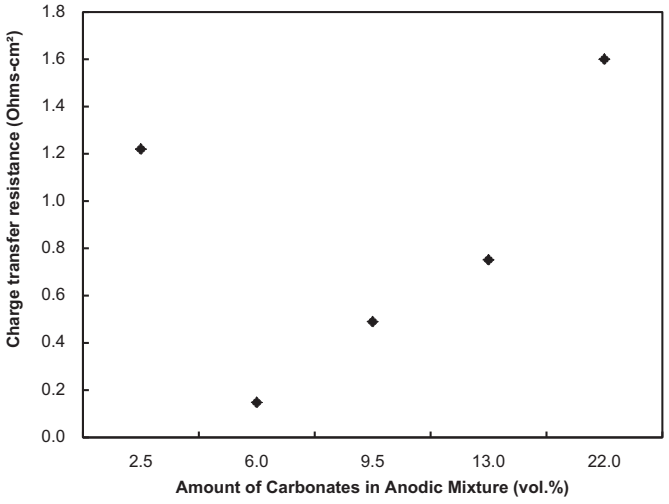


**Fig. 9.** Charge transfer resistance in the anode of the cells using the different volume fractions of carbonate within the anodic mixture (2.5, 6, 9.5, 13, 22) at 800 °C. These cells were tested with carbon black as the fuel in the anodic mixture, Li–K carbonates and dense/porous GDC layers as the anode structure.

transfer resistance nearly tripled (~0.75 Ω cm$^2$) and the power density dropped to ~38 mW cm$^{-2}$ (at 800 °C). The increase in anode polarization followed a nearly linear trend with the increase in carbonate loading between 6 and 22 vol % carbonates. At the high 22 vol % carbonate loading, the charge-transfer resistance increased to ~1.6 Ω cm$^2$ and displayed a lower power density (5 mW cm$^{-2}$) at 800 °C than that achieved by the fuel cell without carbonate addition. Interestingly, the change in temperature for this high carbonate loading had little effect on the overall performance (as shown in Fig. 8). With respect to the carbonate percolation within the fuel feed, these loadings above the threshold composition resulted in the formation of a liquid phase within the anode chamber, which altered the reaction mechanism (solid/liquid mechanism). In addition, the progressive increase in the liquid phase (with increased carbonate addition) would further increase the diffusion distance, and thus, increase fuel diffusional limitations (concentration polarization resistance). This was seen with the appearance of a Warburg element above the percolation threshold. As the carbonate addition increases, the carbon percolation will decrease, which also has an effect on the current collection. Side experiments completed in this work showed that when the Pt current collector wire/mesh were removed from the surface of the cell and placed within the bulk carbonate/carbon mixture, the power showed little change at low carbonate contents. At the higher carbonate contents, the power decreased, potentially due to the lower percolated network of carbon which assists in electron movement to the current collector.

### 3.3. Alternate anode/carbonate systems

The most common carbonate system investigated for the DCFC is either the Li–K–Na carbonate eutectic or various Li–K carbonate compositions [1,42–44,13,14]. A systematic comparison among alternative possible carbonate systems at a composition below the carbonate/carbon percolation limit has not been shown [44]. Alternative carbonate systems were tested at the 6 vol % carbonate loading level (94 vol % carbon black fuel). The carbonate compositions investigated were Li–Na, Li–Na–K, Li–Ba, and Na–K using their eutectic compositions (melting points 498, 398, 609, and 709 °C, respectively) [28,29]. The particle size of all the precursor carbonates was in the same size range as the Li carbonate precursors discussed above. In addition, the OCV of all compositions was quite similar in most cases (with the average near 1.15 ± 0.1 V (at 800 °C) and 1.0 ± 0.05 V (at 700 °C)). The Li–Ba carbonate mixture presented the lowest OCV (0.95 V at 700 °C). The maximum performance of the cells with different compositions of carbonates is shown in Fig. 10 for various temperatures. Typically, DCFC researchers are interested in altering the carbonate composition in order to lower the DCFC operating temperature, which is dictated by the melting temperature of the eutectic. Also, by choosing a carbonate composition with a lower melting temperature, the viscosity of the solution may be reduced which would enhance solid diffusion throughout the medium. In the case of this experiment, the probability for the presence of a liquid phase is minimal, thus these above considerations may be minimized. Of prime importance is the catalytic effect of the cations in the electrochemical oxidation of the carbon fuel. Na appears to have a negative effect on the performance of the cells. With the replacement of the Li–Na binary, the power density of the DCFC decreased 50% and 30% at 700 and 800 °C, respectively, compared to the Li–K carbonate binary. Alternatively, the addition of K significantly affected the performance. Potassium is known to have a strong catalytic effect for carbon oxidation [45] Interestingly, the Li–Na–K eutectic showed an even further decrease in performance to 18 mW cm$^{-2}$ and 45 mW cm$^{-2}$ at 700 and 800 °C, respectively,

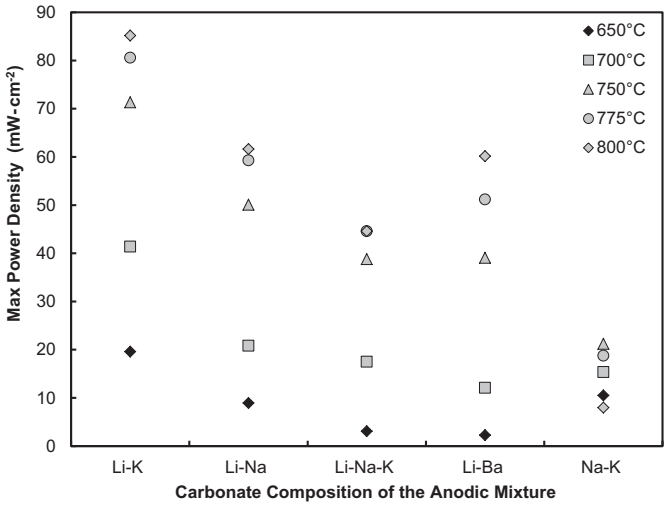


**Fig. 10.** Maximum power density of the cells using the different carbonate compositions (Li–K, Li–Na, Li–Na–K, Li–Ba, Na–K). These cells were tested using dense/porous GDC layers as the anode structure and a carbonate composition of 6 vol% in the anodic mixture.

which is in contrast to the higher performance of the Li–K carbonate binary. Lithium enhanced the potassium's catalytic effect as shown by the comparison between the Li–K and Na–K carbonate samples. Na and K displayed a lower catalytic effect among all the compositions tested, with the maximum powder densities between 7.5 and 10.5 mW cm$^{-2}$ at 650–800 °C. The alkaline-earth ion, barium, was also investigated as a replacement for Na and K alkali ions. In addition, molten carbonate fuel cells have previously utilized Ba carbonate as an additive to control degradation rates of the refractory containers [46]. In this work, the Li–Ba eutectic showed similar performance to the Li–Na system at 800 °C, but the performance at the lower temperatures was slightly reduced compared to the Li–Na system. In the end, the Li–K binary system displayed the highest power density at all temperatures.

## 4. Conclusions

A direct carbon fuel cell with a multi-layered LSCF cathode and an YSZ electrolyte was fabricated and tested using different anode catalyst microstructures/compositions, anode carbonates, and fuel-mixture ratios. Initial experiments focused upon the use of a low fraction (6 vol %) of Li–K carbonate within the fuel mixture. This work incorporated carbon black as the baseline fuel source. It was found that GDC screen-printed on the anode side of the electrolyte greatly improved the performance of the cell and aided the electrochemical reaction. The presence of a porous/dense GDC bi-layer on the electrolyte/anode interface resulted in a significant decrease in the anode polarization resistance and increase in cell performance. A dense GDC layer alone also improved the power density over a bare YSZ electrolyte interface. These results have been observed through the *V–I–P* measurements at various temperatures and confirmed with the anode polarization resistance data measured by EIS. With the same dry carbonate loading within the fuel (6 vol % carbonate–94 vol % carbon black), the Li–K carbonate system displayed the highest power densities over the alternative carbonate mixtures (Li–Na, Li–Na–K, Li–Ba, and Na–K) tested in this work.

The work also investigated the effect of the carbonate-to-carbon ratio within the anode compartment. By reviewing previous research on the DCFC, it was noticed most researchers incorporate a dry carbonate/carbon fuel mixture into the fuel cell. In most of these works, the carbon fuel was not added directly into the already

molten carbonate anode. The current work followed a similar procedure of adding a premixed solid charge to the DCFC. Therefore, depending upon the particle size and packing density of carbonate/carbon mixture within the anode compartment, a specific carbonate percolation threshold must be exceeded before a molten anode could be formed at typical testing temperatures. In this work, the percolation threshold was found to be ~9 vol % (considering hexagonal packing); thus, the carbonate additions below this threshold would persist as the solid carbonate. In this case, the reaction mechanism within the DCFC anode compartment would be dominated by a purely solid/solid reaction (solid electrolyte to carbon) or a CO oxidation reaction similar to that of a SOFC (solid/gas reaction), where a liquid phase would not participate in the electrochemical reaction. The carbonates acted more as a catalyst for the carbon oxidation at or near the electrolyte interface. Also, the carbonate compositions below the percolation threshold did not show the large diffusional limitations as seen when a large volume of liquid phase is present in the anode compartment at carbonate compositions above the percolation threshold.

## Acknowledgments

The authors would like to thank Fundacion Caja Madrid (Spain), WVU Advanced Energy Initiative (AEI) program, and Dr. Ever Barbero for their financial support of this program. The authors would also like to acknowledge Ms. Adrienne MacLeod for assistance with SEM and Ms. Anna McClung for electrochemical testing.

## References

[1] C. Jiang, J. Irvine, Journal of Power Sources 196 (2011) 7318–7322.
[2] S. Ansolabehere, The Future of Coal: Options for a Carbon-Constrained World, Massachusetts Institute of Technology, Boston MA, 2007. ISBN 978-0-615-14092-6.
[3] European Commission Staff Working Document, Biomass Action Plan, COM (2005) 628 Final, 7 December 2005.
[4] IEO 2011, U.S. Energy Information Administration, International Energy Outlook 2011. DOE/EIA-0484 (September 2011). Washington, DC.
[5] A. Jolley, Climate Change Project Working Paper Series No 8, Advanced Technologies Applicable to Fossil Fuels: Cross-cutting Technologies and Carbon Capture/Storage, Center for Strategic Economic Studies at Victoria University, Australia, March 2006.
[6] S. Jain, Y. Nabae, B. Lakeman, D. Pointon, J. Irvine, Solid State Ionics 179 (2008) 1417–1421.
[7] G. Hackett, J. Zondlo, R. Svensson, Journal of Power Sources 168 (2007) 111–118.
[8] M. Dresselhaus, Basic Research Needs For The Hydrogen Economy" A Report from the Basic Energy Sciences Workshop on Hydrogen Production, Storage, and Use. Available at: (May 2003) (last accessed 10.10.12) http://www.sc.doe.gov/bes/hydrogen.pdf.
[9] W. Clark, J. Rifkin, T. O'Connor, J. Swisher, T. Lipman, G. Rambach, Utilities Policy 13 (2005) 41–50.
[10] M. Ball, M. Wietschel, International Journal of Hydrogen Energy 347 (2009) 615–627.
[11] S. Zecevic, E. Patton, P. Parhami, Carbon 42 (2004) 1983–1993.
[12] R.H. Wolk, S. Lux, S. Gelber, F.H. Holcomb, September 2007, Direct Carbon Fuel Cells: Converting Waste to Electricity, ERDC-CERL TR-07–32, U.S. Army Engineer Research and Development Center Construction Engineering Research Laboratory (ERDC-CERL).
[13] X. Li, Z. Zhu, R. Marco, J. Bradley, A. Dicks, Journal of Power Sources 195 (2010) 4051–4058.
[14] D. Cao, Y. Sun, G. Wang, Journal of Power Sources 167 (2007) 250–257.
[15] Y. Nabae, K. Pointon, J. Irvine, Journal of the Electrochemical Society 156 (6) (2009) B716–B720.
[16] Fuel Cell Handbook, seventh ed., EG&G Technical Services, Inc. U.S. Department of Energy, November 2004, pp. 2.10–2.17.
[17] J. Lijun, T. Ye, L. Qinghua, X. Chun, Y. Jinshuai, W. Zhiming, Y. Li, Y. Zhaoa, Journal of Power Sources 195 (2010) 5581–5586.
[18] H. Li, Q. Liu, Y. Li, Electrochimica Acta 55 (2010) 1958–1965.
[19] N.J. Cherepy, R. Krueger, K.J. Fiet, A.F. Jankiwski, J.F. Cooper, Journal of The Electrochemical Society 152 (1) (2005) A80–A87.
[20] M. Chen, C. Wang, X. Niu, S. Zhao, J. Tang, B. Zhu, International Journal of Hydrogen Energy 35 (2010) 2732–2736.
[21] Y. Tang, J. Liu, International Journal of Hydrogen Energy 35 (2010) 11188–11193.
[22] C. Li, Y. Shi, N. Cai, Journal of Power Sources 195 (2010) 4660–4666.
[23] M. Dudek, P. Tomczyk, Catalysis Today 176 (1) (2011) 388–392.
[24] H. Ju, S. Uhm, J. Kim, R. Song, H. Choi, S. Lee, J. Lee, Journal of Power Sources 198 (2012) 36–41.
[25] T. Tao, W. Mcphee, M. Koslowske, L. Beteman, M. Slaney, J. Bentley, ECS Transactions 12 (2008) 681–690.
[26] T. Tao, W. McPhee, M. Koslowske, J. Bentley, M. Slaney, L. Beteman, ECS Transactions 25 (2) (2009) 1115–1124.
[27] Y.D. Zhen, A.I.Y. Tok, S.P. Jiang, F.Y.C. Boey, Journal of Power Sources 178 (2008) 69–74.
[28] http://www.sgte.org/fact/documentation/FTsalt/FTsalt_Figs.htm (last accessed 10.10.12).
[29] G. Janz, M. Lorenz, Journal of Chemical and Engineering Data 6 (3) (1961) 321–323.
[30] P. Gansor, C. Xu, K. Sabolsky, J.W. Zondlo, E.M. Sabolsky, Journal of Powers Sources 198 (2012) 7–13.
[31] K. Haberko, M. Jasinski, P. Pasierb, M. Radecka, M. Rekas, Journal of Power Sources 195 (2010) 5527–5533.
[32] G. Corre, G. Kim, M. Cassidy, J.M. Vohs, R.J. Gorte, J.T.S. Irvine, Chemistry of Materials 21 (2009) 1077–1084.
[33] J. Wade, C. Lee, A. West, K. Lackner, Journal of Membrane Science 369 (2011) 20–29.
[34] M. Benamira, A. Ringuedé, L. Hildebrandt, C. Lagergren, R. Vannier, M. Cassir, International Journal of Hydrogen Energy 37 (24) (2012) 19371–19379.
[35] M. Benamira, A. Ringuedé, V. Albin, R.-N. Vannier, L. Hildebrandt, C. Lagergren, M. Cassir, Journal of Power Sources 196 (13) (2011) 5546–5554.
[36] An Introduction To Electrochemical Impedance Measurement, Solartron Analytical, Technical Report No. 6. http://www.korozja.pl/html/eis/technote06.pdf. (last accessed 10.10.12).
[37] D. Pletcher, R. Greff, R. Peat, L.M. Peter, Instrumental Methods in Electrochemistry, Horwood Publishing, 2001. University of Southampton (Chapter 8) ISBN: 1-898563-80-2.
[38] C.L. Zeng, W. Wang, W.T. Wu, Corrosion Science 43 (2001) 787–801.
[39] L. Jia, Y. Tian, Q. Liu, C. Xia, J. Yu, Z. Wang, Y. Zhao, Y. Li, Journal of Power Sources 195 (17) (2010) 5581–5586.
[40] J.F. Cooper, J.R. Selman, International Journal of Hydrogen Energy (2012), http://dx.doi.org/10.1016/j.ijhydene.2012.03.095.
[41] A. Malliaris, D.T. Turner, Journal of Applied Physics 42 (1971) 614–618.
[42] A. Kornhauser, R. Agarwal, Modeling and Design for a Direct Carbon Fuel Cell with Entrained Fuel and Oxidizer, DE-FG26–03NT41801, Department of Mechanical Engineering, Virginia Polytechnic Institute and State University, April, 2005.
[43] D. Cao, G. Wang, C. Wang, J. Wang, T. Lu, International Journal of Hydrogen Energy 35 (2010) 1778–1782.
[44] A.C. Rady, S. Giddey, S.P.S. Badwal, B.P. Ladewig, S. Bhattacharya, Energy Fuels 26 (2012) 1471–1488.
[45] X. Wu, L. Radovic, Carbon 43 (2005) 333–344.
[46] H. Ohzu et al, United States Patent 4,895,774. 23, January 1990.